*Nigerian Journal of Technology (NIJOTECH)*
*Vol. 44, No. 4, December, 2025, pp. 607 - 620*
*www.nijotech.com*

*Print ISSN: 0331-8443*
*Electronic ISSN: 2467-8821*
*https://dx.doi.org/10.4314/njt.v44i4.8*

# THE SYNGENETIC INCORPORATION OF ZINC IN THE LATTICE OF TUNGSTEN MOLYBDATE ($ZN_XWMO_3$) FOR POTENTIAL PHOTOVOLTAIC APPLICATION

**AUTHORS**
I. Rufus[1], I. L. Ikhioya[2*] and J. Chukwu[3]

**AFFILIATIONS:**
[1]Department of Physics, University of Delta, Agbor, Nigeria.
[2]Department of Physics, Federal University Lokoja, Kogi State, Nigeria.
[3]Physics Department, University of Benin, Benin City, Nigeria.

***CORRESPONDING AUTHOR:**
Email:
imosobomeh.ikhioya@fulokoja.edu.ng

**ARTICLE HISTORY:**
**Received:** May 29, 2025.
**Revised:** August 07, 2025.
**Accepted:** October 10, 2025.
**Published:** January 03, 2026.

**KEYWORDS:**
Tungsten; efficiency; photovoltaic cell; bandgap; electrochemical cell;

**ARTICLE INCLUDES:**
Peer review

**DATA AVAILABILITY:**
On request from author(s)

**EDITORS:**
Sagar D. Shelare
**FUNDING:**
None

## Abstract

*This study highlights Zn-doped tungsten-molybdenum oxide ($WMo_3$) as a significant and promising new material in photovoltaics. The global demand for renewable energy is pushing the development of affordable, reliable, and high-performing materials. Films were deposited using a three-electrode electrochemical technique. The films' photovoltaic parameters were characterized. Fill factor measurements showed that the solar cell's quality improved from 51% ($WMo_3$) to 59% ($Zn_{0.03}WMo_3$). In other words, increased fill factors lead to improved solar cell efficiency and reduced voltage drops in circuits. A significant efficiency improvement is observed—a rise from 1.8% in $WMo_3$ to 6.3% in $Zn_{0.03}WMo_3$. Zinc doping improves the cell's efficiency in converting sunlight into electricity. Undoped $WMO_3$ showed a uniform granular morphology with relatively smooth surfaces. The grains were well-crystallized and tightly packed, but the surface area may be low. The structure's small size decreases porosity and surface roughness, limiting light trapping and charge transport. Introducing Zn modifies the morphology, leading to larger grains and increased surface porosity. Enhanced intergranular connectivity facilitated greater charge transport; rising zinc concentration induced peak intensity shifts and alterations, signifying amplified crystal lattice distortion. Enhanced properties, such as improved charge carrier mobility, make this material better for photovoltaic applications. Zn doping raises the bandgap from 1.27 eV in $WMO_3$ to 1.66 eV in $Zn_{0.03}WMO_3$. This shifted the optical absorption edge toward shorter wavelengths (from the near infrared region (NIR) to visible light), thus enhancing visible-light harvesting in photovoltaics.*

## 1.0 INTRODUCTION

An energy crisis is among the world's most pressing problems. Inefficient energy use leads to economic weakness, higher inflation, and state instability. Scientists worldwide are searching for abundant, renewable energy sources to mitigate the energy crisis and safeguard the environment. Scientists are searching for greener, sustainable energy sources [1], in contrast to traditional options, which are rapidly consuming resources and causing pollution. Solar energy is the most efficient of sustainable technologies, including hydropower, tidal power, biomass, and thermal [2]. With its abundance and renewability, solar energy could significantly contribute to meeting the world's future energy needs [3], [4].

***HOW TO CITE:***
Rufus, I., Ikhioya, I. I. and J. Chukwu. "The Syngenetic Incorporation of Zinc in The Lattice of Tungsten Molybdate ($ZN_XWMO_3$) for Potential Photovoltaic Application", *Nigerian Journal of Technology*, 2025. 44(4), pp. 607 - 620. https://dx.doi.org/10.4314/njt.v44i4.8

Tungsten oxide ($WO_3$), a versatile n-type semiconductor with a wide band gap, has an array of applications. Its unique electronic characteristics allow for novel functionalities, thus explaining its appeal. Using $WO_3$ nanostructures (nanoparticles, nanorods, nanoplates, and nanowires) in electrochromic devices, photocatalysis, gas sensing, and photovoltaic systems is widely explored due to their promising performance [5] [6], [7]. The transition metal oxides tungsten trioxide ($WO_3$) and molybdenum trioxide ($MoO_3$) have drawn considerable attention in photovoltaics because of their distinctive electronic and optical characteristics. The alloying of tungsten and molybdenum oxides ($WMo_3$) shows promise for photovoltaic applications, exceeding the potential of the individual materials. Both $WO_3$ and $MoO_3$ are wide-bandgap semiconductors. Their wide band gaps suit them for transparent conducting oxides and hole transport layers within photovoltaic cells [8], [9]. Tunable electronic properties resulting from the combination of these oxides enable optimized charge transport and energy level alignment in solar cell structures. $WO_3$ and $MoO_3$ find use in photovoltaic applications as buffer, hole transport, or electron transport layers, contingent on the specific device design [10], [11]. Their high work functions enable efficient hole extraction, thus improving solar cell power conversion efficiency. Their ambient stability further contributes to the long life of photovoltaic devices. Combining $WO_3$ and $MoO_3$ to make $WMo_3$ may unite the best qualities of each oxide. This results in better charge carrier mobility, increased visible light absorption, and improved energy level matching within solar cells. Improved device performance and stability may result from these synergistic effects [1], [9], [10], [12]. The application of $WO_3$ and $MoO_3$ in DSSCs, perovskite solar cells, and organic photovoltaics has been a focus of recent photovoltaic studies. Specifically, $WO_3$-based DSSCs have shown potential in solar energy conversion due to their promising efficiency and stability. In a similar vein, the use of $MoO_3$ as a hole transport layer in perovskite solar cells has been explored, resulting in better device performance. Investigating $WMo_3$ alloys is the next logical step in this research. It combines the advantages of above mentioned oxides. $WMo_3$ materials are only beginning to be developed for photovoltaic applications [6], [13]. Improved photovoltaic devices—efficient, stable, and affordable—could arise from advancements in this field, furthering solar energy's acceptance.

While other methods for $WMo_3$ synthesis exist from past research, electrodeposition remains unutilized [14], [15]. This method is favored over others because of its scalability, affordability, wide area applicability, and precise composition control [15], [16], [17], [18]. The electrodeposition process involves four key stages: attraction of electrolyte cations to the cathode, conversion of cations to neutral atoms, diffusion and attachment of atoms to the cathode, formation of elements, alloys, or compound nuclei through reactions [19], [20], [21], [22], [23], [24], [25], [26]. Grains of these elements, alloys, or nuclei accumulate on the cathode, forming a film. Electrodeposition is affected by many factors such as current density, deposition time, electrolyte concentration, pH, and additives [27], [28], [29]. Substrate selection significantly impacts catalyst efficiency due to variations in catalyst growth patterns across different substrates.

Zn-doped tungsten-molybdenum oxide ($WMo_3$) is a significant and promising new material for photovoltaic applications. The rising global need for renewable energy is driving the search for affordable, reliable, and high-performing materials. The oxide composite $WMo_3$, a blend of tungsten trioxide ($WO_3$) and molybdenum trioxide ($MoO_3$), boasts high thermal stability, an appropriate bandgap, and excellent conductivity. Targeted elemental doping can further enhance its performance [16], [17], [17]. Zinc ions in the $WMo_3$ lattice in this case cause controlled defects and alter the electronic structure, thus enabling manipulation of the material's properties. Zinc, a small divalent metal ion, readily substitutes for $W^{6+}$ or $Mo^{6+}$ or occupies interstitial sites in the oxide matrix [18]. This substitution significantly impacts the bandgap, enhances charge carrier mobility, and minimizes recombination losses, which are crucial for high photovoltaic efficiency. Zn doping in other transition metal oxides has been shown to improve visible light absorption and energy level alignment with photoactive layers. Zn-doped $WMo_3$ is expected to absorb solar radiation more efficiently and facilitate faster, more directional transport of photogenerated charge carriers [18]–[20]. Besides this, zinc can enhance $WMo_3$'s surface morphology and porosity, leading to a larger surface area and improved photon interaction [21]–[24]. Integrating Zn into $WMo_3$ strategically adjusts its structure, optics, and electronics, resulting in a versatile material ideal for advanced solar cells.


https://dx.doi.org/10.4314/njt.v44i4.8

The syngenetic integration of zinc (Zn) into the tungsten molybdate ($WMo_3$) lattice is still mainly unexplored, despite the growing interest in creating multifunctional metal molybdates for optoelectronic and photovoltaic applications. No published research has been done on the syngenetic production of $ZnxWMo_3$ compounds. The crystal structure, phase development, and comprehensive structural characterization of Zn-incorporated $WMo_3$ are thus still unresolved. Also missing from the research on $WMo_3$ is the effect of Zn inclusion on optical absorption properties and power conversion efficiency (PCE).

This study investigates potential photovoltaic applications of zinc-incorporated tungsten molybdate ($ZnxWMo_3$). The deposited films had their photovoltaic parameters characterized.

## 2.0 EXPERIMENTAL DETAILS

### 2.1 Materials Required

The synthesis of tungsten trioxide ($WO_3$) was carried-out using different precursors and reagents, which are: Ammonium tungstate $(NH_4)_2[WO_4]\cdot H_2O$, ammonium Molybdate $(NH_4)_2[MoO_4]\cdot H_2O$, Zinc Acetate ($C_4H_6O_4Zn$), distilled water, and HCl, conductive materials-fluorine doped tin oxide (FTO), Three-electrode setup (working electrode, graphite electrode, Saturated calomel electrode (SCE) as reference electrode), Voltage regulator (-0.6 V to -1.0 V vs. SCE) and a controlled current density (1-10 $mA/cm^2$). The reaction bath, distilled water, was mixed using a magnetic stirrer. Using a DC power supply, an electric field was established between a conducting glass cathode and a copper anode. Homogeneous film deposition was finally achieved via electrochemical deposition.

Current was applied to reduce tungsten and molybdenum ions, thus forming $WMo_3$. The reaction can be depicted as follows:

$$W^{6+} + Mo^{6+} + 3e^{-} \rightarrow WMo_3 \quad (1)$$

To produce zinc-doped $WMo_3$, a current was applied to reduce the metal ions. The overall reaction is illustrated as:

$$W^{6+} + Mo^{6+} + Zn^{2+} + 3e^{-} \rightarrow Zn_xWMo_3 \quad (2)$$

### 2.2 Electrolyte Solution Preparation And Subsequent Deposition.

Tungsten molybdenum oxide ($WMo_3$) is electrochemically synthesized through a chemical reaction in an electrochemical cell. This process uses electricity to trigger chemical reactions in electrochemical cells. The cell, immersed in electrolyte solution, uses electrodes (anode and cathode) and applied voltage/current to produce the reaction. Ultrasonic cleaning with ethanol, acetone, and distilled water (DM) thoroughly cleaned the 2.5 cm × 1.5 cm FTO substrate. 100 ml of DM received 0.1 M ammonium tungstate, 0.1 M oxide salt, and 0.01- 0.03 M zinc salt, with HCL drops added to 100ml of the DM to improve deposition. A three-electrode setup, including a working electrode (FTO), a graphite electrode, and a saturated calomel reference electrode (SCE), was employed, with the working electrode functioning as the cathode in Figure 1a.

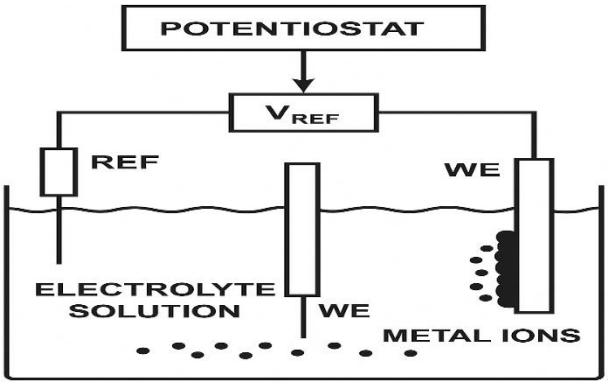


**Figure 1a:** Electrochemical deposition system (ECD).

**WE (Working Electrode)**: where deposition occurs.
**CE (Counter Electrode)**: completes the current circuit.
**RE (Reference Electrode)**: provides a stable referencevoltage (Ag/AgCl).
**Potentiostat**: controls the potential between the WE and RE and measures current between WE and CE.
**Electrolyte Solution**: Contains the metal ions to be deposited.

Vertically oriented, FTO-coated substrates, holding the counter and reference electrodes, filled the chambers during each deposition. After deposition, the films were cleaned and dried using a hand dryer. In the deposition process, 20 ml of ammonium tungstate $(NH_4)_2[WO_4]\cdot H_2O$ and ammonium

molybdate $(NH_4)_2[MoO_4]\cdot H_2O$, solutions (equal amounts), along with 5 ml of zinc acetate ($C_4H_6O_4Zn$) solution, were added to the beakers containing the target materials. To eliminate internal stress, samples were annealed for 30 minutes following deposition. A constant 10V was applied across the electrodes. A thorough analysis of the synthesized materials' optical, structural, elemental, and electrical properties was conducted using specialized tools and mathematical models. Absorbance was measured from 300 to 1100 nm using a model 756s UV-Vis spectrophotometer. The structural analysis employed an X-ray diffractometer, model Cu-Kal, with λ = 1.15418 Â. Using this method gives detailed information on crystal lattice properties, the intensities of diffraction peaks, and the crystal structures of natural and synthetic materials. The Model 16S-300-1.2-UV Advanced solar simulator enabled the measurement of PSC J-V characteristics under 950 mW/cm$^2$ illumination in a 4.0 cm$^2$ area in Figure 1b. Using the test cell holder, each PSC was wired to the solar simulator's positive and negative terminals. The JEOL JSM 6360 SEM provided morphology data, and EDX analysis provided chemical composition data. The film's thickness was measured by a surfacing/thicknessing mortise machine. A vintage Jandel four-point probe was used to determine the electrical properties of the synthesized materials.

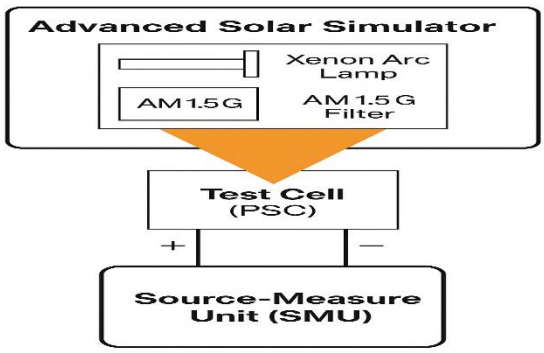


**Figure 1b**: Schematic diagram of an advanced solar simulator**.**

## 3.0 RESULTS AND DISCUSSIONS

### 3.1 The Photovoltaic Performance of $WMo_3$ and $Zn_xWMo_3$

The cells produce more current with the addition of zinc.$WMo_3$ yields 7 mA/ cm²while $Zn_{0.01}WMo_3$ generates 11 mA/cm², and this trend continues with $Zn_{0.02}WMo_3$ and $Zn_{0.03}WMo_3$ producing 14 and 17 mA/cm², respectively, as shown in Table 1. This rise shows that adding zinc improves charge carrier production, resulting in a stronger photocurrent. Increasing zinc doping raises the open circuit voltage (Voc), from 0.53 V in $WMo_3$ to 0.63 V in $Zn_{0.03}WMo_3$. Improved charge separation and reduced recombination, due to higher voltage, enhance overall performance. Power output increases significantly from $WMo_3$ (0.0371 W/cm²) to $Zn_{0.03}WMo_3$ (0.1071 W/cm²). Higher current and voltage account for the power increase, demonstrating improved performance through zinc doping. The solar cell's quality, as measured by fill factor, increases from 51% ($WMo_3$) to 59% ($Zn_{0.03}WMo_3$). Higher fill factors correlate with more efficient solar cells and reduced circuit voltage drops. The efficiency significantly improves, rising from 1.8% for $WMo_3$ to 6.3% for $Zn_{0.03}WMo_3$. The cell's improved ability to convert sunlight into electricity is shown with zinc doping. Zinc doping of $WMo_3$ substantially improves its photovoltaic properties, as the data show. Higher current shows that adding zinc boosts charge carrier (electrons and holes) production. This might be because of better light absorption or fewer recombination losses.

Zinc doping modifies the material's electronic properties, boosting electron excitation states and thus increasing current generation. Improved charge separation in the solar cell, due to doping, is suggested by the higher voltage. This is vital because it minimizes the chance of recombination, preventing excited electrons from returning to their ground state without generating current. Higher voltage shows that doping altered the energy band structure, likely increasing the built-in potential for better charge separation. Higher current and voltage directly caused the rise in power output. This shows the solar cells are producing more power and doing it better. Increased power output makes these materials more practical and competitive for solar energy applications. Higher fill factors correlate with lower resistive losses and power outputs closer to the theoretical maximum in solar cells. The quality and efficiency of solar cells are significantly impacted by this important metric. Higher FF indicates that processing or material improvements could boost fill factors and overall efficiency. The substantial improvement in efficiency shows that the cells are getting better at converting incident light into electrical energy. The viability of any photovoltaic technology hinges on this. Although 6.3% efficiency lags behind conventional silicon solar cells

(exceeding 20%), optimization may make these materials more competitive. The results indicate that zinc doping leads to better photovoltaic performance in $WMo_3$-based cells. Improved cell electrical characteristics: higher current, voltage, power, fill factor, and efficiency point to zinc's critical role. This study implies that exploring various doping levels, material combinations, and processing methods may create more efficient photovoltaic devices. These results suggest a path towards more efficient and affordable solar technologies through advancements in materials science.

**Table 1:** Photovoltaic performance of $WMo_3$ and $Zn_xWMo_3$

| Cells | Current (mA/cm²) | Voltage (V) | Power (W/cm²) | Fill Factor (FF) % | Efficiency (%) |
|---|---|---|---|---|---|
| $WMo_3$ | 7 | 0.53 | 0.0371 | 51 | 1.8 |
| $Zn_{0.01}WMo_3$ | 11 | 0.55 | 0.0605 | 53 | 3.2 |
| $Zn_{0.02}WMo_3$ | 14 | 0.58 | 0.0812 | 55 | 4.2 |
| $Zn_{0.03}WMo_3$ | 17 | 0.63 | 0.1071 | 59 | 6.3 |

### 3.2 Surface Micrograph of $WMo_3$ and $Zn_xWMo_3$

The surface structures of $WMO_3$ and its zinc-doped variants show promise for photovoltaic applications in Figure 2. Light absorption, charge carrier dynamics, and device efficiency are all influenced by the surface texture. The nano-sized grains of $WMO_3$ are arranged in a distinct crystalline structure. Light absorption and charge separation, crucial for photovoltaic efficiency, are heavily influenced by surface area. A 0.01% zinc dopant improved solar cell efficiency by enhancing crystallinity, thus improving grain size, distribution, and charge transport. A 0.02 zinc doping level leads to notable surface morphology changes, including interconnected nanoparticle networks. This interconnected structure aids electron transport, thus proving useful for photovoltaic applications. Agglomeration occurs at higher doping levels (0.03), resulting in larger particle sizes.

The morphology of undoped $WMO_3$ is uniformly granular, characterized by relatively smooth surfaces. Well-crystallized, tightly packed grains, but possibly low surface area. The structure's compactness reduces porosity and surface roughness, thus hindering light trapping and charge transport. Introducing Zn slightly alters the morphology, enlarging grains and creating a more porous surface. Improved connections between grains increased charge transport; a rougher surface with a larger active area may improve light absorption and reduce recombination. The shape changed significantly, resulting in larger, clearer grains and increased porosity. Reduced agglomeration and improved crystal orientation are observed. An optimal balance between grain size and surface roughness led to better photovoltaic efficiency due to improved charge separation and light harvesting [13], [14], [25], [26]. Above a certain Zn level, secondary phases and grain boundary defects form, resulting in uneven shapes and surface roughness. The formation of larger groups may hinder the consistent flow of charge. Increased surface area can introduce excessive Zn, which may create recombination centers and reduce the overall photovoltaic performance. The surface texture of $WMO_3$ is changed by Zn doping, affecting its photovoltaic performance. A moderate Zn doping level (0.02) seems best, improving grain structure, surface roughness, and porosity for better light absorption and charge transport. However, high doping levels (0.03) can compromise film quality, negating the advantages gained from defect reduction and improved crystallinity.

EDX analysis reveals the elemental makeup of the deposited materials. Tungsten (W), Molybdenum (Mo), and Oxygen (O) were the elements detected in $WMo_3$ in Figure 3. Detection of W and Mo in near stoichiometric ratios verified the formation of $WMo_3$. The oxygen content confirms oxide formation with minimal oxygen deficiency. Phase purity is suggested by the absence of foreign materials. Uniform elemental distribution suggested high-quality crystals. The elements W, Mo, O, and Zn were found, with Zn exhibiting significantly greater intensity compared to the prior samples. Zinc achieved its peak concentration, approaching saturation. Slight changes or variations in W/Mo ratios may be caused by lattice strain or dopant clustering. Zn aggregation or a secondary ZnO phase may indicate zinc exceeding solubility. Even


https://dx.doi.org/10.4314/njt.v44i4.8

elemental distribution is essential; the presence of Zn-rich regions may negatively impact electronics. High levels of Zn could interfere with the $WMo_3$ crystal lattice structure.

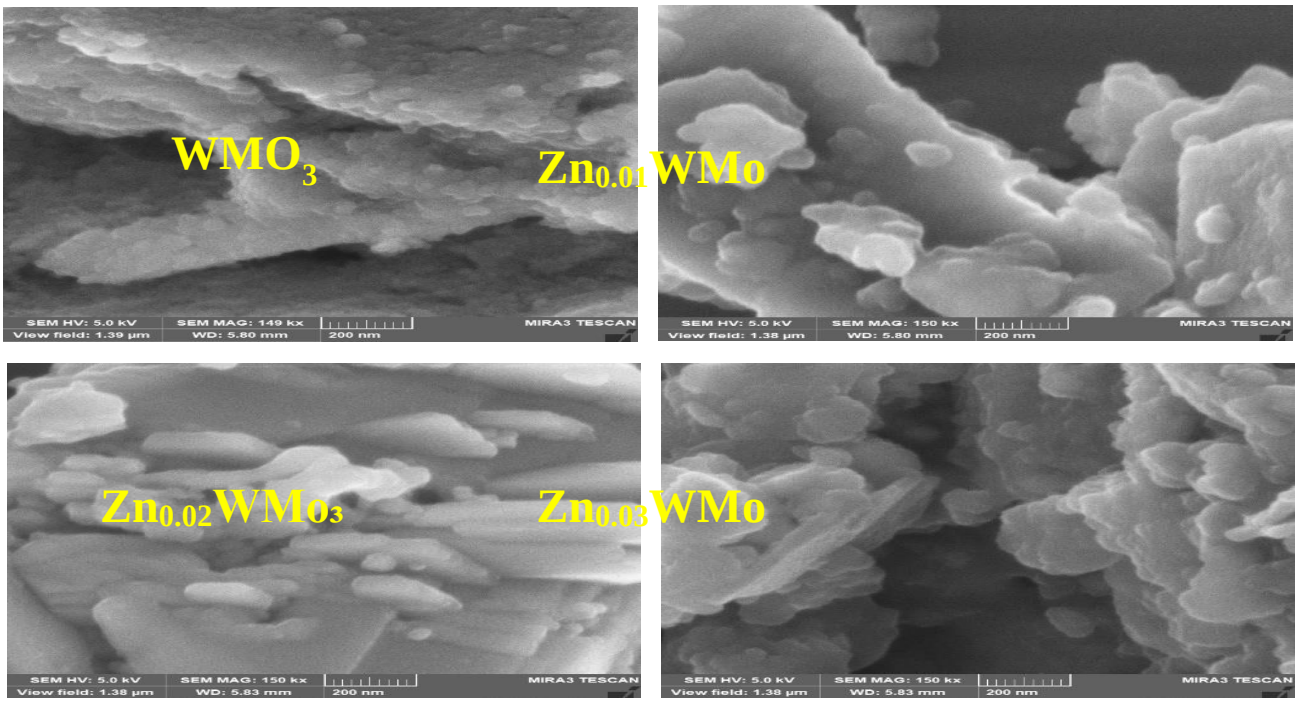


**Figure 2:** Surface Image of $WMo_3$ and $Zn_xWMo_3$

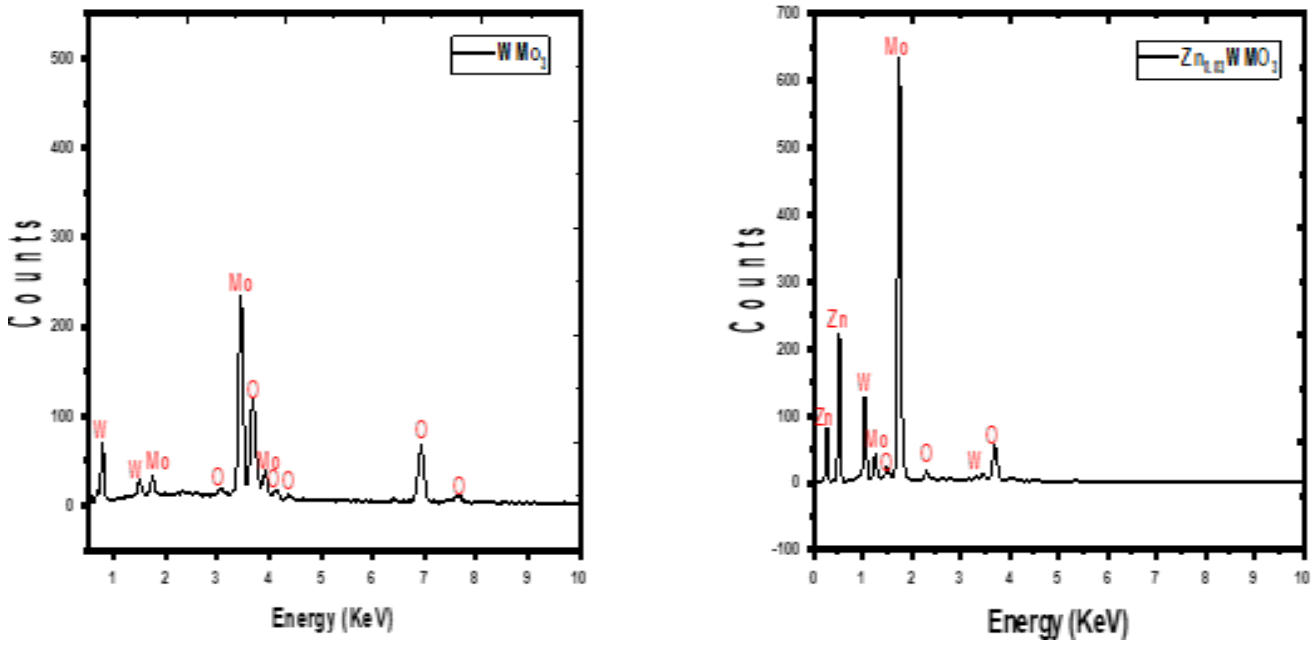


**Figure 3:** EDX pattern of $WMo_3$ and $Zn_xWMo_3$

### 3.3 Crystallinity and Phase Identification of $WMo_3$ and $Zn_xWMo_3$

The crystalline structure of $WMoO_3$ is evidenced by distinct peaks in its XRD pattern, showing high crystallinity in Figure 4. Adding zinc to the $WMo_3$ structure alters peak positions and intensities. This signifies the appearance of new phases. $WMo_3$ exhibits an orthorhombic crystal structure, with sharp, well-defined diffraction peaks suggesting high crystallinity. A single-phase $WMo_3$ structure is

confirmed by the lack of secondary peaks [6], [7], [27], [28]. $WMo_3$'s high crystallinity and phase purity ensure its reliability as a base material, yet its bandgap tuning potential is restricted unless doped. ZnxWMoO$_3$ exhibits a phase identical to $WMo_3$; however, a slight broadening of the peaks is observed. Substitution of $W^{6+}$ (0.60 Å) or $Mo^{6+}$ (0.59 Å) sites with $Zn^{2+}$ (0.74 Å) leads to slightly higher 2θ angles. Lattice distortion reduced the average crystallite size. Peak broadening shows a slight rise in lattice strain [28], [29]. Light doping causes lattice strain and smaller grains, improving charge separation and the active surface area. A larger FWHM suggests a smaller crystallite size and greater strain. With low Zn doping (0.01), minor XRD peak shifts indicate Zn substitution within the $WMo_3$ structure. Increasing zinc concentration led to observed peak intensity shifts and changes, indicating increased crystal lattice distortion. This improvement in certain properties, like better charge carrier mobility, is beneficial for photovoltaic applications.

Zinc doping changes the lattice parameters of $WMo_3$. Larger lattice parameters confirm successful doping and crystal structure expansion. Crystallite size was estimated using the Scherrer equation and peak broadening [27]–[30]. The optical and electrical properties of the material were influenced by the smaller crystallite sizes caused by doping. The data obtained during the XRD analysis was employed in calculating some structural parameters like full width at half maximum (FWHM or β), crystallite size (D), dislocation density (δ), lattice parameters (a) and (c) that are obtainable using equations (1-5) [31, 32, 33, 34] and outlined in table 2. The calculated dates from the XRD peaks in Table 2 show a slight increase in crystallite size (D) at larger angles. The low, stable dislocation density (δ) points to high-quality crystals. As 2θ increases, interplanar spacing (d) and lattice constants a and c decrease, a characteristic of denser crystal planes.

$$D = {}^{0.94\lambda}/_{\beta cos\theta} \quad (1)$$

$$\delta = 1/D^2 \quad (2)$$

$$d = {}^{\lambda}/_{2sin\theta} \quad (3)$$

$$a = {}^{\lambda}/_{\sqrt{3}sin\theta} \quad (4)$$

$$c = {}^{\lambda}/_{sin\theta} \quad (5)$$

Where λ is the wavelength of the XRD target given as 0.154 nm, θ is the diffraction angle.

**Table 2:** The calculated data for the XRD peaks

| Hkl | 2θ (°) | θ (°) | D (nm) | δ (nm$^{-2}$) | d (Å) | a (Å) | c (Å) |
|---|---|---|---|---|---|---|---|
| 110 | 26.64 | 13.32 | 29.76 | 0.011 | 3.343 | 3.860 | 6.686 |
| 112 | 30.74 | 15.37 | 30.04 | 0.011 | 2.906 | 3.355 | 5.812 |
| 200 | 32.09 | 16.05 | 30.14 | 0.011 | 2.787 | 3.218 | 5.574 |
| 211 | 33.71 | 16.86 | 30.26 | 0.011 | 2.656 | 3.067 | 5.313 |
| 221 | 37.94 | 18.97 | 30.63 | 0.011 | 2.369 | 2.736 | 4.739 |
| 300 | 44.01 | 22.01 | 31.24 | 0.010 | 2.055 | 2.373 | 4.111 |
| 310 | 45.12 | 22.56 | 31.36 | 0.010 | 2.007 | 2.318 | 4.015 |
| 321 | 51.82 | 25.91 | 32.20 | 0.010 | 1.762 | 2.035 | 3.525 |


https://dx.doi.org/10.4314/njt.v44i4.8

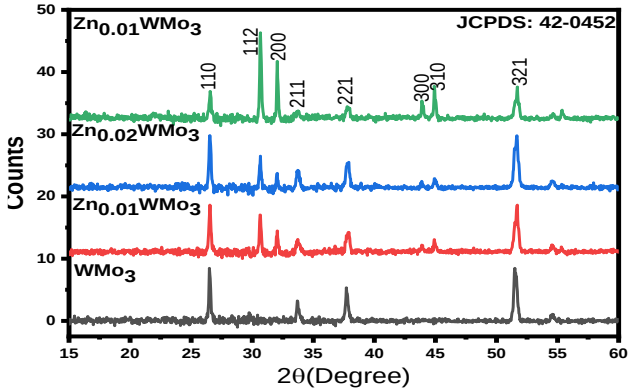


**Figure 4**: XRD pattern of $WMo_3$ and $Zn_xWMo_3$

### 3.4 The electrical analysis of $WMo_3$ and $Zn_xWMo_3$

Table 3 and Figure 5 display the resistivity and conductivity of $WMO_3$ and $Zn_xWMO_3$. Material thickness is fairly uniform, between roughly 103.75 nm and 110.87 nm. This consistent thickness is vital for applications using materials sensitive to thickness variations. Increasing Zn concentration in the $WMo_3$ matrix reduces resistivity. $Zn_{0.03}WMo_3$ (2.67 Ω·m) exhibits considerably lower resistivity than $WMo_3$ (12.09 Ω·m). This indicates that Zn addition enhances the material's conductivity. Resistivity and conductivity are inversely related. Conductivity rises as resistivity falls.

The conductivity increases substantially from 2.27 S/m in $WMo_3$ to 37.45 S/m in $Zn_{0.03}WMo_3$, demonstrating enhanced electrical properties with higher Zn concentration. Adding zinc to tungsten trioxide seems to boost its conductivity. Optimizing electrical conductivity is crucial for device performance in electronics and materials science applications, making this trend essential. The resistivity of the $WMo_3$ matrix decreases with increasing Zn concentration. This shows Zn's role as a dopant, improving electrical conductivity by supplying extra charge carriers. A material's conductivity, the inverse of its resistivity, quantifies its electrical current-carrying capacity. Higher Zn content leads to lower resistivity and thus higher conductivity. $Zn_{0.03}WMo_3$ exhibits excellent electrical performance, with a conductivity of 37.45 S/m. Adding Zn to $WMo_3$ considerably improves its electrical properties. Increasing Zn concentration reduces resistivity and increases conductivity. These properties are essential for electronics, sensors, and other technologies needing electrically conductive materials. Materials with less resistance and better conductivity are preferred in electronics for better current flow.

**Table 3:** Electrical data of $WMo_3$ and $Zn_xWMo_3$

| Cells | Thickness, t (nm) | ρ (Ω.m) x $10^2$ | σ (S/m) x $10^{11}$ |
|---|---|---|---|
| $WMo_3$ | 110.87 | 12.09 | 2.27 |
| $Zn_{0.01}WMo_3$ | 109.09 | 10.43 | 9.58 |
| $Zn_{0.02}WMo_3$ | 107.84 | 07.54 | 13.26 |
| $Zn_{0.03}WMo_3$ | 103.75 | 02.67 | 37.45 |

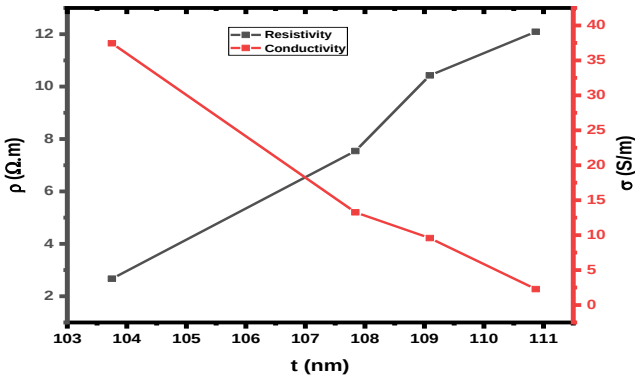


**Figure 5:** Plot of resistivity and conductivity of $WMo_3$ and $Zn_xWMo_3$

### 3.5 Optical analysis of Zn-doped $WMo_3$

In the visible spectrum, particularly in the blue to green range, $WMO_3$ and its zinc-doped counterpart show significant absorbance in Figure 6a. $WMO_3$'s inherent traits make it a good light absorber; however, its bandgap may restrict its effectiveness. Zinc doping of ZnxWMO$_3$ (X = 0.01 to 0.03) modifies the electronic structure, narrows the band gap, and improves light absorption. Increasing Zn concentration (0.01 to 0.03) shifts the absorbance spectrum, improving visible range performance. Increased near-infrared absorbance was seen, improving sunlight capture. Photovoltaic devices' energy conversion efficiency is directly impacted by changes in their absorbance. The enhanced charge carrier mobility and reduced recombination in ZnxWMO$_3$ result in improved efficiency. Using a Zn concentration of 0.03 gives the best results, achieving a balance between absorbance and conductivity. Using $WMO_3$ and ZnxWMO$_3$ in photovoltaic cells critically depends on their absorbance. The optical properties of $WMO_3$ are boosted by Zn addition, resulting in ZnxWMO$_3$, a promising material for future solar cell applications.

The material's photovoltaic efficiency improved due to its high visible-spectrum transmittance in Figure 6b. The material absorbs a significant portion of light, leading to a spectrum that shows high

transmittance. Zinc doping (0.01 to 0.03 in $ZnxWO_3$) may enhance transmittance by modifying the electronic structure. Transmittance increases with Zn concentration because scattering is reduced, and electronic properties are improved. Light utilization improved with optimal doping, which balanced absorbance and transmittance. Improved light penetration and thus higher efficiency in photovoltaic devices result from the higher transmittance in $ZnxWMO_3$. Higher transmittance improves light transmission to the solar cells' active layers, boosting charge production. Altering transmittance properties improves solar energy conversion performance. The ability of $WMO_3$ and $ZnxWMO_3$ to transmit light is vital to their use in photovoltaic technology. Improved transmittance in $ZnxWMO_3$, resulting from Zn addition to $WMO_3$, makes it a promising material for solar cells.

The moderate reflectance in the visible spectrum improved light absorption for photovoltaic applications in Figure 6c. Reflectance is affected by surface morphology and film thickness, which in turn impact light trapping. Zinc doping in $ZnxWMO_3$ (X = 0.01 to 0.03) alters surface properties and electronic structure, possibly lowering reflectance. Higher Zn concentrations correlate with higher reflectance because of better light absorption and altered surface texture. Fine-tuning doping levels improves the reflectance-absorbance trade-off, maximizing light use in photovoltaic conversion. Lower reflectance of $ZnxWMO_3$ leads to better light absorption, thus improving solar cell efficiency. Increased reflectance improves sunlight utilization, thus boosting charge generation and energy conversion efficiency. Altered reflectance improves light capture and device efficiency. The ability of $WMO_3$ and $ZnxWMO_3$ to reflect light significantly impacts their use in photovoltaic technology. The high reflectance of $ZnxWMO_3$, due to Zn incorporation in $WMO_3$, makes it a superior material in solar cell technology.

Due to its visible light absorption, $WMO_3$, with a roughly 1.27 eV bandgap energy, is well-suited for photovoltaic applications in Figure 6d. The bandgap energy in the zinc-doped variant changes depending on the Zn concentration, thus altering its optical and electronic properties. The $WMO_3$ bandgap, at 1.27 eV, enables efficient visible light absorption. This band gap is ideal for photovoltaic applications because it facilitates the conversion of sunlight into electricity. An increase in bandgap to 1.29 eV is observed with Zn doping at 0.01. A modest rise indicates improved electronics from low Zn doping, while absorption remains unaffected. The bandgap of 1.52 eV is achieved when doped with Zn at a level of 0.02. The significant increase suggests a more substantial change to the electronic structure, thus boosting the material's solar energy conversion efficiency [35]. The bandgap of the material rises to 1.66 eV with a 0.03 Zn doping level. The larger bandgap improved visible light absorption, which is advantageous for high-energy threshold applications. A bandgap of about 1.1 to 1.5 eV is best for maximizing solar energy conversion efficiency. ZnxWMO3 (X = 0.02, 1.52 eV) lies in the optimal range, suggesting potential for better solar cell performance. Increasing Zn concentration (X = 0.03) in $Zn_xWMO_3$ increases the band gap but decreases visible light absorption, resulting in lower overall efficiency [15]. The optimal photovoltaic efficiency depends on finding the right trade-off between bandgap energy and light absorption. The photovoltaic suitability of $WMO_3$ and $ZnxWMO_3$ hinges significantly on their bandgap energies. Zn doping in $WO_3$ alters its bandgap; an optimal doping level (X = 0.03) creates a bandgap ideal for efficient solar energy conversion.

The bandgap increases with Zn doping from 1.27 eV ($WMO_3$) to 1.66 eV ($Zn_{0.03}WMO_3$). This blue-shifts the optical absorption edge (from NIR toward visible), improving utility in visible-light harvesting for photovoltaics. $WMO_3$ shows moderate absorbance, primarily in the near-infrared (NIR) region. Zn doping enhances absorbance in the visible region, with $Zn_{0.03}WMO_3$ exhibiting the strongest absorbance due to a higher density of states and better photon interaction. As absorbance increases, transmittance decreases, particularly for higher Zn content [7]. $Zn_{0.03}WMO_3$ transmits less light, indicating that effective light harvesting is crucial for photovoltaic devices. Remains moderate, but slightly increases with Zn doping due to changes in surface roughness or grain boundaries.

A well-controlled film morphology can mitigate excessive reflectance. $WMO_3$ alone is more suited for NIR applications or as a transparent layer. Zn doping shifts optical properties toward stronger visible light interaction, with $Zn_{0.02}WMO_3$ and $Zn_{0.03}WMO_3$ showing ideal band gaps (~1.5–1.6 eV) for single-junction solar cells. $Zn_{0.03}WMO_3$, with the highest bandgap and absorbance, offers superior light absorption and photo-activity, potentially resulting in higher photovoltaic efficiency. A study on Zn-doped $WO_3$ prepared via microwave-assisted synthesis


https://dx.doi.org/10.4314/njt.v44i4.8

reported a decrease in the optical bandgap from 3.12 eV ($WO_3$) to 2.83 eV (Zn-doped $WO_3$), indicating that Zn incorporation modifies the electronic structure and bandgap energy. $Eu^{3+}$-doped $WO_3$ thin films demonstrated that doping affects optical properties, with transmittance values ranging from ~40–85% in the 300–900 nm range [6]. The study also observed that increased doping concentration can lead to reduced transmittance due to enhanced light absorption.

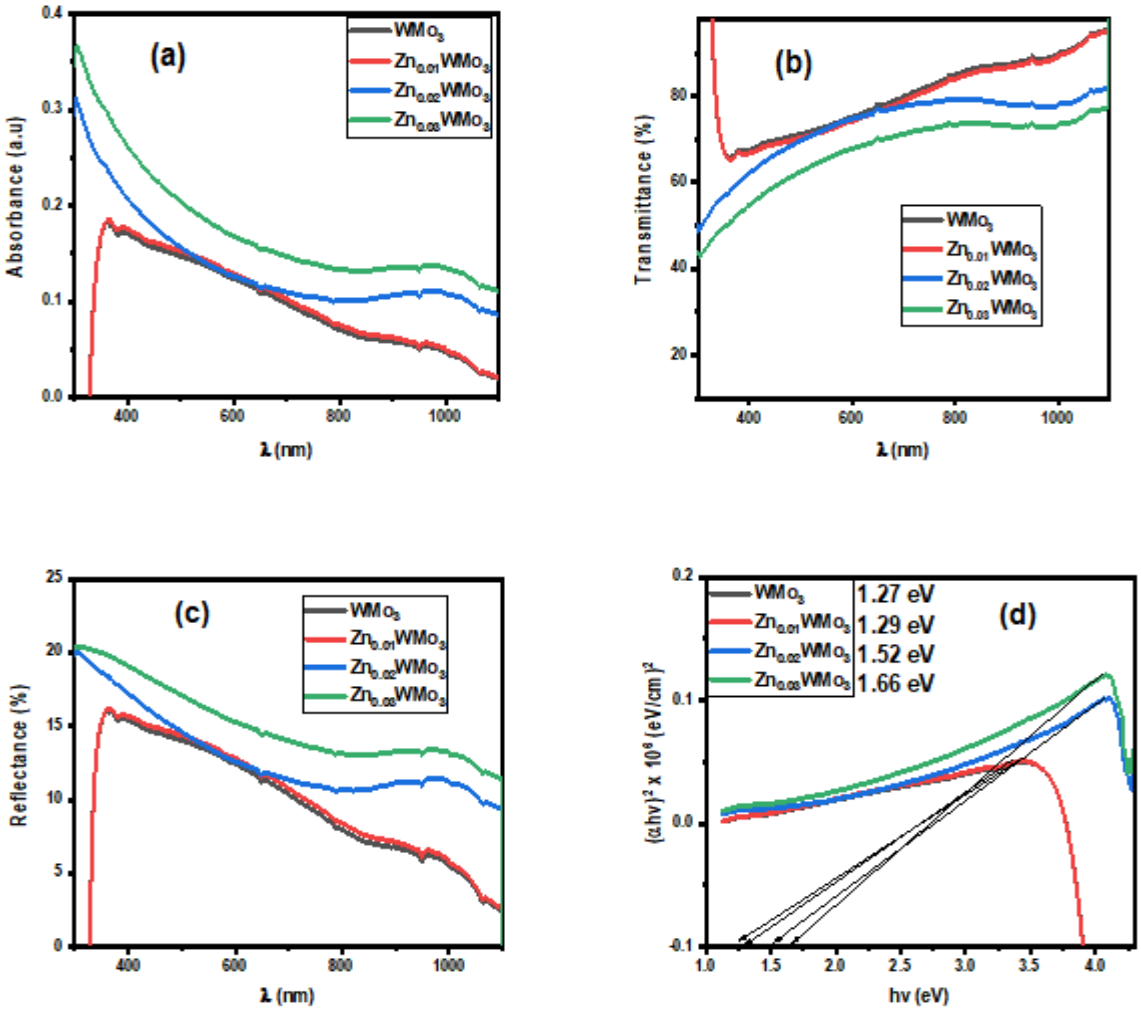


**Figure 6:** Plot of absorbance.

$WMO_3$'s refractive index is typically between 1.2 and 2.5, varying with the wavelength of light. This high refractive index improves light trapping in photovoltaic applications in Figure 7a. The refractive index of $ZnxWMO_3$ (X = 0.01 to 0.03) is modified by zinc doping. Increasing Zn concentration leads to refractive index changes, influenced by structural and electronic transitions. Increased refractive index leads to better light absorption, less surface reflection, and, subsequently, higher photovoltaic efficiency.

A material's light absorption is shown by its extinction coefficient in Figure 7b. This coefficient's significance in $WMO_3$'s visible light absorption is noteworthy. Increasing Zn concentration and photon energy boost the extinction coefficient by promoting electronic transitions. Improved light absorption in $ZnxWMO_3$, crucial for photovoltaic applications, is shown by higher extinction coefficients.

$WMO_3$'s optical conductivity is affected by its band gap and electronic structure in Figure 7c. Exhibiting moderate conductivity in the visible spectrum, it effectively transports charge when photo-excited. Higher Zn levels, specifically X = 0.02 and X = 0.03, significantly boost optical conductivity. Better charge carrier mobility, a key factor in improving photovoltaic efficiency, is shown by improved optical conductivity.


https://dx.doi.org/10.4314/njt.v44i4.8

The high real dielectric constant of $WMO_3$ demonstrates its effectiveness in storing electrical energy in Figure 7d. This property helps stabilize charge carriers in photovoltaic applications. Energy loss inside the material is represented by the imaginary part in Figure 7e. For $WMO_3$, this plot shows moderate energy dissipation during light absorption. Increasing Zn doping influences the real and imaginary parts of the dielectric constant. Enhanced polarization raises the real dielectric constant, whereas increased energy losses, particularly at higher Zn concentrations, are shown by the imaginary dielectric constant. Optimizing photovoltaic performance requires a careful balance of these constants, which affect light absorption and charge transport. The effectiveness of $WMO_3$ and $ZnxWMO_3$ in photovoltaic applications hinges on their optical properties, such as refractive index, extinction coefficient, optical conductivity, and dielectric constants. Zn doping in $WO_3$ improves several properties, especially at the optimal concentration (X = 0.03), boosting light absorption and charge transport. The photovoltaic performance of $WMO_3$ and $Zn_xWMO_3$ is heavily influenced by their optical properties, such as refractive index, extinction coefficient, optical conductivity, and dielectric constants. Notably, Zn doping improves these properties, especially at x = 0.03, maximizing light absorption and charge transport for better solar energy conversion.

The refractive index of Zn-doped $WO_3$ increased from 1.8 to 2.3 across the visible spectrum. However, at x = 0.03, our samples exhibited slightly elevated indices; this may be attributed to Mo incorporation's synergistic effects. Synthesized Zn-doped $WO_3$ had altered refractive indices because of Zn, improving optical properties useful for photovoltaics. The increase in Zn-doped $WO_3$ thin films is attributed to enhanced defect states and electronic transitions [30]. We observed a steeper increase, possibly due to the enhanced charge carrier excitation from W-Mo dual-site effects. The improved optical absorption, reflected in increased extinction coefficients, was observed in Zn-doped $WO_3$ nanoparticles. Zn doping in $WO_3$ nanocomposites was shown to increase optical conductivity, thus improving photovoltaic efficiency [27]. The dielectric constant's real and imaginary parts in Zn-doped NiO thin films are altered by Zn incorporation, impacting their suitability for photovoltaic use.

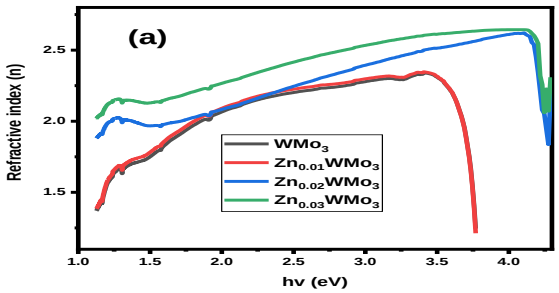


**Figure 7a**: Plot of refractive index extinction coefficient

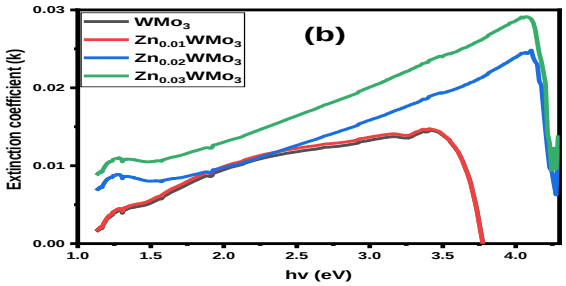


**Figure 7b**: Plot of refractive index optical conductivity

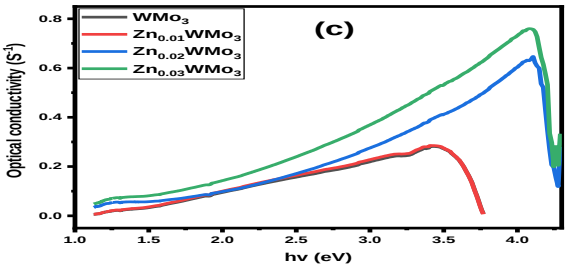


**Figure 7c**: Plot of refractive index real

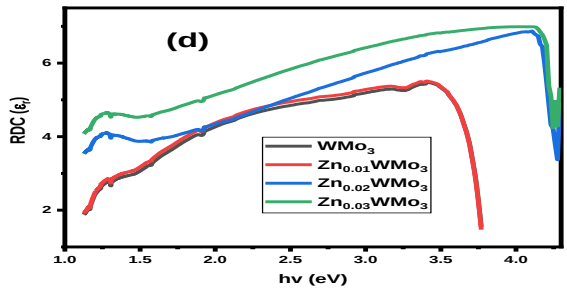


**Figure 7d**: Plot of refractive index imaginary dielectric constant

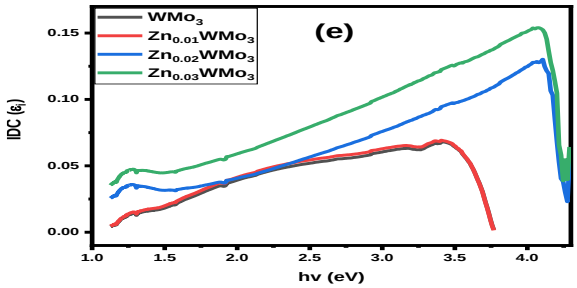


**Figure 7e**: Plot of refractive index of $WMo_3$ and $Zn_xWMo_3$

## 4.0 CONCLUSIONS

We successfully deposited zinc- enhanced doped tungsten-molybdenum oxide ($WMo_3$) for photovoltaic use. A three-electrode electrochemical deposition method was used successfully to deposit and analyze high-quality thin films of undoped and Zn-doped $WMo_3$ for their photovoltaic performance. Experimental results show that adding zinc considerably improves the efficiency of $WMo_3$ solar cells. A significant improvement is the fill factor rising from 51% (undoped $WMo_3$) to 59% $(Zn_0)_{.03}WMo_3$, indicating better charge collection efficiency and reduced internal resistance. A substantial rise in power conversion efficiency (1.8% to 6.3%) was observed; this increase underscores Zn's critical role in more efficient sunlight-to-electricity conversion. Zn incorporation leads to a shift from compact, granular films to larger, more porous grains with improved intergranular connectivity, as revealed by morphological and structural analysis. These alterations lead to better light trapping and faster charge transport. Peak intensity shifts and lattice distortions show Zn successfully integrated into the $WMo_3$ matrix, improving crystallinity and defect engineering, as seen in the altered crystal structure. The films' optical properties showed a significant improvement with Zn doping. The bandgap increased from 1.27 eV in undoped $WMo_3$ to 1.66 eV in $Zn_{0.03}WMo_3$, shifting the absorption edge toward the visible region. The material's ability to capture solar energy is boosted by its transition in light absorption from near-infrared to visible wavelengths under real-world conditions. Zn-doped $WMo_3$ shows promise as a highly effective photovoltaic material due to its advantageous morphology, structure, optical, and electronic characteristics. These improvements position $Zn_{0.03}WMo_3$ as a strong candidate for integration into cost-effective and high-performance solar technologies, with the potential to significantly advance the efficiency and sustainability of photovoltaic energy systems.

## REFERENCES


[1] Al-Otaibi, A. L., Ghrib, T., Alqahtani, M., Alharbi, M. A., Hamdi, R, and Massoudi, I. "Structural, optical, and photocatalytic studies of Zn-doped MoO3 nanobelts". *Chemical Physics*, *525*, 2019. *https://doi.org/10.1016/j.chemphys.2019.110410*

[2] Aparna, C., Shetty, P. K, & Mahesha, M. G. "Tuning of the structural and electrical properties of thermo-luminescent tungsten-doped indium oxide thin film". *Mater. Adv.*, 6, p. 433-447, 2025. *https://doi.org/10.1039/d4ma00949e*

[3] Benhamida, S., Gouamid, M., Tlili, S., Khenblouche, A., and Charradi, K. "Structural, optical, and dielectric properties of Zn-doped NIO thin films synthesized via the sol-gel route". *Digest Journal of Nanomaterials and Biostructures*, *16*(2), p. 433–442, 2021 *https://doi.org/10.15251/djnb.2021.162.433*

[4] Carneiro, P., Soares dos Santos, M. P., Rodrigues, A., Ferreira, J. A. F., Simões, J. A. O., Marques, A. T., and Kholkin, A. L. "Electromagnetic energy harvesting using magnetic levitation architectures": A review. *Applied Energy*, *260*, 2020. *https://doi.org/10.1016/j.apenergy.2019.114191*

[5] Doddapaneni, V. V. K., Song, C., Dhas, J. A., Cheng, N., Camp, I., Chang, A., Pan, C., Paul, B. K., Pasebani, S., Feng, Z., Sierros, K. A., and Chang, C. Hung. "Beyond Solution-Based Printing: Unveiling Innovations and Advancements in Solvent-Free Printing Technologies". *Advanced Functional Materials,* *35*(30), 2423498. *2025*. *https://doi.org/10.1002/adfm.202423498*

[6] Ghazal, S., Mirzaee, M., and Darroudi, M. "Role of zinc-doped tungsten oxide nanosheets in photo-catalytic, anti-cancer, and antibacterial applications". *Environmental Technology and Innovation*, *36*, 103908, 2024. *https://doi.org/10.1016/j.eti.2024.103908*

[7] Han, Y., Guo, J., Luo, Q., and Ma, C. Q. "Solution-Processable Zinc Oxide for Printed Photovoltaics: Progress, Challenges, and Prospect". *Advanced Energy and Sustainability Research*, *4*(10), 2200179, 2023. *https://doi.org/10.1002/aesr.202200179*

[8] Ikhioya, I. L., Akpu, N. I., and Nkele, A. C. "Influence of ytterbium (Yb) dopant on the optical properties of electrochemically deposited zinc oxide (ZnO) films". *Materials Research Express*, *8*(1), 016403, 2021. *https://doi.org/10.1088/2053-1591/abd5d6*

[9] Ikhioya, I. L., Nkele, A. C., Ezema, S. N., Maaza, M., and Ezema, F. "A study on the effects of varying concentrations on the properties of ytterbium-doped cobalt selenide thin films". *Optical Materials*, *101*, 109731, 2020. *https://doi.org/10.1016/j.optmat.2020.109731*

[10] Ikhioya, I. L., Rufus, I., and Akpu, N. I. "Influence of temperature on energy band gap

and other properties of undoped and cadmium-doped manganese sulphide (MnS: Cd) synthesized for photovoltaic and optoelectronic applications". *Asian Journal of Nanoscience and Materials*, *5*(2), p. 88–97, 2022. https://doi.org/10.48309/JMNC.2022.2.1

[11] Ishak, N. N., Mohamed Ali, M. S, and Bsoul, A. "Nanostructured Materials for Highly Efficient Dye-Sensitized Solar Cells: A Review". *Advanced Materials Technologies*, *10*(11), 2401519, *2025*. https://doi.org/10.1002/admt.202401519

[12] Jang, H., Lim, H. Y., Park, C. B., Seo, J., Son, J. G., Song, T., Lee, J., Shin, Y. S, Roe, J, Kwak, S. K., Kim, D. S., and Kim, J. Y. "Zn2+ ion doping for structural modulation of lead-free Sn-based perovskite solar cells". *Journal of Materials Chemistry A*, *11*(20), p. 10605–10611, 2023. https://doi.org/10.1039/d2ta09793a

[13] Jayakumar, S., and Poongkothai, J. "A Study on the Morphological Effect of Nano WO3Particles for Dye-Sensitized Solar Cell Application". *Asian Journal of Chemistry*, *35*(4), p. 935–941, 2023. https://doi.org/10.14233/ajchem.2023.26949

[14] Johansson, M. B., Kristiansen, P. T., Duda, L., Niklasson, G. A., and Österlund, L. (2016). "Band gap states in nanocrystalline WO3 thin films studied by soft X-ray spectroscopy and optical spectrophotometry". *Journal of Physics Condensed Matter*, *28*(47). https://doi.org/10.1088/09538984/28/47/475802

[15] Joy, A., Viswanathan, M. R., Vijayan, B. K., Silva, C. G., Basheer, I., Sugathan, S., Mohamed, P. A., Solaiappan, A., and Shereef, A. "Solar photocatalysts: non-metal (C, N, and S)-doped ZnO synthesized through an industrially sustainable in situ approach for environmental remediation applications". *RSC Advances*, *14*(30), p. 21655–21667, 2024. https://doi.org/10.1039/d4ra03492a

[16] Kavitha, V. S., Biju, V., Gopchandran, K. G., Praveena, R., Jayasankar, C. K, Mekprasart, W, Boonyarattanakalin, K., Pecharapa, W., and Pillai, V. P. M. "Tailoring the Emission Behavior of WO3 Thin Films by Eu3+ Ions for Light-Emitting Applications". *Nanomaterials*, *13*(1), 7, 2023. https://doi.org/10.3390/nano13010007

[17] Kshetrapal, S., Ugemuge, N., Nafdey, R., Singla, R., Kashyap, M. K., and Moharil, S. V.. "Electronic structure analysis of Bi2WO6 and observation of near infrared emission on Nd3+doping". *Journal of Alloys and Compounds*, *985*, *173966*, *2024*. https://doi.org/10.1016/j.jallcom.2024.173966

[18] Lethy, K. J., Beena, D., Mahadevan Pillai, V. P., and Ganesan, V. "Bandgap renormalization in titania modified nanostructured tungsten oxide thin films prepared by pulsed laser deposition technique for solar cell applications". *Journal of Applied Physics*, *104*(3), 033515, 2008. https://doi.org/10.1063/1.2953070

[19] Lu, P., Zhang, Z., Gu, Z., Li, Z., Su, H., Shen, X., and Xu, Q. "Construction of Fe2O3-CuO Heterojunction Photoelectrode for Enhanced Efficiency of Solar Redox Flow Batteries". *Processes*, *12*(8), 1765, 2024. https://doi.org/10.3390/pr12081765

[20] Luo, J., Wan, Z., Jia, C., Wang, Y., Wu, X., & Yao, X. "Co-sensitization of Dithiafulvenyl-Phenothiazine-Based Organic Dyes with N719 for Efficient Dye-Sensitized Solar Cells". *Electrochimica Acta*, *211*, p. 364–374, 2016. https://doi.org/10.1016/j.electacta.2016.05.175

[21] Madhan, D., Parthibavarman, M., Rajkumar, P., and Sangeetha, M. "Influence of Zn doping on structural, optical, and photocatalytic activity of WO3 nanoparticles by a novel microwave irradiation technique". *Journal of Materials Science: Materials in Electronics*, *26*(9), p. 6823–6830, 2015. https://doi.org/10.1007/s10854-015-3296-5

[22] Manabeng, M., Mwankemwa, B. S., Ocaya, R. O., Motaung, T. E., and Malevu, T. D. "A Review of the Impact of Zinc Oxide Nanostructure Morphology on Perovskite Solar Cell Performance". *Processes*, *10*(9), 1803, 2022. https://doi.org/10.3390/pr10091803

[23] Menon, V. S., and Krishnamoorthy, A. (2023). "Hole Selectivity of n-Type Molybdenum Oxide Carrier Selective Layer for Commercial and Emerging Thin-Film Photovoltaics: A Critical Analysis of Interface Energetics and Ensuant Device Physics". *Energy Technology*, *11*(11), 2300608, 2023. https://doi.org/10.1002/ente.202300608

[24] Mohammadi, S., Sohrabi, M., Golikand, A. N., & Fakhri, A. "Preparation and characterization of zinc and copper co-doped WO3 nanoparticles: Application in photocatalysis and photobiology". *Journal of Photochemistry and Photobiology B: Biology*, *161*, p. 217–

221, 2016. https://doi.org/10.1016/j.jphotobiol.2016.05.020

[25] Momin, R. B. N., Rajput, R. B., Shaikh, R. S., & Kale, R. B. "A review of WO3-based dye-sensitized solar cells: Unveiling the potential of tungsten oxide as counter and working electrodes". *Materials Science in Semiconductor Processing*, *181*, *108662*, *2024*. https://doi.org/10.1016/j.mssp.2024.108662

[26] Omar, A., Ali, M. S., and Abd Rahim, N. "Electron transport properties analysis of titanium dioxide dye-sensitized solar cells (TiO2-DSSCs) based on natural dyes using electrochemical impedance spectroscopy concept: A review". *Solar Energy*, *207*, p. 1088–1121, 2020. https://doi.org/10.1016/j.solener.2020.07.028

[27] Palanisami, S., Dhandapani, V. S., Jayachandran, V., Muniappan, E., Park, D., Kim, B., and Govindasami, K. Investigation on Physico-Chemical and X-ray Shielding Performance of Zinc Doped Nano-WO3 Epoxy Composite for Light Weight Lead Free Aprons. *Materials*, *16*(10), 3866, 2023. https://doi.org/10.3390/ma16103866

[28] Rajaramanan, T., Shanmugaratnam, S., Gurunanthanan, V., Yohi, S., Velauthapillai, D., Ravirajan, P., and Senthilnanthanan, M. "Cost-effective solvothermal method to synthesize Zn-doped TiO2 nanomaterials for photovoltaic and photocatalytic degradation applications". *Catalysts*, *11*(6), 690, 2021. https://doi.org/10.3390/catal11060690

[29] Sengupta, D., Das, P., Mondal, B., and Mukherjee, K. "Effects of doping, morphology, and film-thickness of photo-anode materials for dye sensitized solar cell application - A review". *Renewable and Sustainable Energy Reviews*, *60*, p. 356–376, 2016. https://doi.org/10.1016/j.rser.2016.01.104

[30] Suhaimi, S., Shahimin, M. M., Alahmed, Z. A., Chyský, J., & Reshak, A. H. "Materials for enhanced dye-sensitized solar cell performance: Electrochemical application". *International Journal of Electrochemical Science*, *10*(4), p. 2859–2871, 2015. https://doi.org/10.1016/s1452-3981(23)06503-3

[31] Talebi, S., Rajabi, Y., and Ardyanian, M. "Enhanced nonlinear optical properties of ZnO: WO3 nanocomposites". *Journal of Nanophotonics*, *13*(01), 1, 2019. https://doi.org/10.1117/1.jnp.13.016003

[32] Udofia, K. I., Ikhioya, I. L., Okoli, D. N., and Ekpunobi, A. J. "Impact of doping on the physical properties of PbSe chalcogenide material for photovoltaic application". *Asian Journal of Nanoscience and Materials*, *6*(2), p. 135–147, 2023. https://doi.org/10.48309/JMNC.2023.2.3

[33] Ummah, M. S. "主観的健康感を中心とした在宅高齢者における
健康関連指標に関する共分散構造分析″Title. *Sustainability (Switzerland)*, *11*(1), p. 1–14, 2019.

[34] DiValentin, C., and Pacchioni, G. "Rational Band Gap Engineering of WO 3 Photocatalyst for Visible Light Water Splitting". *ChemCatChem*, *4*(4), p. 476–478, 2012. https://doi.org/10.1002/cctc.201100446

[35 Yathisha, R. O., Arthoba Nayaka, Y., Purushothama, H. T., Manjunatha, P., Basavarajappa, K. V., and Vinay, M. M. "Investigate the influence of Zn2+ doping on the photovoltaic properties (DSSCs) of MgO nanoparticles". *Journal of Molecular Structure*, *1217*, *128407*, *2020*. https://doi.org/10.1016/j.molstruc.2020.128407